Margaret E. Kalacska,[1,2] *Ph.D.; Lynne S. Bell,*[1] *Ph.D.; G. Arturo Sanchez-Azofeifa,*[3] *Ph.D.;*
and Terry Caelli,[4] *Ph.D.*

The Application of Remote Sensing for Detecting Mass Graves: An Experimental Animal Case Study from Costa Rica*

ABSTRACT: Detection of mass graves utilizing the hyperspectral information in airborne or satellite imagery is an untested application of remote sensing technology. We examined the *in situ* spectral reflectance of an experimental animal mass grave in a tropical moist forest environment and compared it to an identically constructed false grave which was refilled with soil, but contained no cattle carcasses over the course of a 16-month period. The separability of the *in situ* reflectance spectra was examined with a combination of feature selection and five different nonparametric pattern classifiers. We also scaled up the analysis to examine the spectral signature of the same experimental mass grave from an air-borne hyper-spectral image collected 1 month following burial. Our results indicate that at both scales (*in situ* and airborne), the experimental grave had a spectral signature that was distinct and therefore detectable from the false grave. In addition, we observed that vegetation regeneration was severely inhibited over the mass grave containing cattle carcasses for up to a period of 16 months. This experimental study has demonstrated the real utility of airborne hyperspectral imagery for the detection of a relatively small mass grave (5 m^2) within a specific climatic zone. Other climatic zones will require similar actualistic modeling studies, but it is clear that the applications of this technology provide the international community with both an early detection tool and a tool for ongoing monitoring.

KEYWORDS: forensic science, remote sensing, mass graves, hyperspectral, tropical environment, spectrometry, decomposition, mammal, human

Human rights violations leading to genocide and crimes against humanity and the subsequent investigation and exhumation of mass graves have received substantial attention over the last decade (1–10). However, consensus not only lacks on who is in charge of the actual exhumation and processing of evidence, but in the recognition of various types of "mass graves" and their definitions (6). Regardless of the definition used to describe these large and complex crime scenes, their existence in numerous countries is gradually being acknowledged even if it is initially denied by the perpetrators.

Millions of people have disappeared in conflicts worldwide; for example, over 200,000 people are conservatively estimated to be missing in Guatemala (1), over 300,000 in Iraq (9), and over 800,000 in Rwanda (4,10). Similar patterns can be seen in other countries, such as East Timor, Sudan, Afghanistan, Argentina, Colombia, Chile, Cambodia, etc. The bodies of victims in these conflicts are frequently buried in mass graves, often clandestine in nature, at various locations within the countries.

Mass graves differ in size from country to country or even within regions. Graves containing groups of two or more individuals to larger discrete graves with 10 to 100 victims have been

reported in Guatemala (1), whereas in other countries, such as Iraq, Bosnia, and Rwanda, mass graves have been found to contain several hundred victims (2–5,9,10). Not all graves are created by the perpetrators; however, bodies may in some cases be recovered by survivors or victims' families and subsequently buried (1). These graves tend to be clandestine and present similar difficulties for accurate detection and recovery.

One of the most successful methods of locating mass graves has been from witness or informant testimony (11), with most cases having suboptimal accuracy, and a large amount of time and resources having been spent on searching for the actual location of the graves. As such, the security of personnel conducting the investigations has become a serious and increasing problem in the timely investigation of mass graves (9). Moreover, by the time a recovery team can assess a scene, the bodies that are recovered are often in various stages of decomposition, complicating or negating positive identification (12).

The working definition of a mass grave by Jessee and Skinner (6) used in this study was "*any location containing two or more associated bodies, indiscriminately or deliberately placed.*" The definition from Jessee and Skinner (6) also elaborates on the context stating that the victims "died as a result of extrajudicial, summary or arbitrary executions." Because our objective is the detection of the graves, the context of victims' death does not preclude other scenarios such as death following a natural catastrophe (e.g., tsunami) or armed conflict. Nevertheless, it is implicit that for the investigation carried out in this study the mass graves involve burial in soil as opposed to other scenarios, such as burial beneath building, in wells, or under water, etc. The study described below is a constrained experimental protocol where a set of grave-filled and grave-empty foci were created to test and explore the utility of remote sensing to this problem. If remote detection has real utility or potential to inform of or observe criminal acts of this kind

[1]School of Criminology, Simon Fraser University, Burnaby, BC, V5A-1S6, Canada.
[2]Department of Geography, McGill University, Montreal, QC, H3A-2K6, Canada.
[3]Earth & Atmospheric Sciences Department, University of Alberta, AB, T6G-2E3, Canada.
[4]National Information and Communication Technology Australia (NICTA), The Australian National University, Canberra, ACT 0200, Australia.

subsequent to the event, then recourse may be made within the context of the criminal code of that country or by the international community. It therefore represents an impartial and important piece of evidence which is secondarily material to the event.

Remote Sensing

The term "remote sensing" has been used to describe a number of tools and technologies. In this study we refer to the discipline of remote sensing from the earth and planetary sciences, and more specifically, the recording and processing of *reflected electromagnetic radiation* in the visible to shortwave infrared wavelengths (13). The recording of the electromagnetic radiation can be achieved at a number of scales with a variety of instruments. Measurements can be "*in situ*" from a field portable spectroradiometer where the data collected are point measurements of reflected radiation. They can also be achieved from an aircraft with an imaging spectroradiometer or from a satellite platform where the resultant data is also in an image form. The concept of the "image" is analogous to a set of stacked photographs where each photograph is only sensitive to a specific narrow range of wavelengths of light; for example, the first photograph would only be sensitive to the 450–465 nm range while the twentieth in the stack only to 735–750 nm, etc. Each layer in the image is digital thus comprising of pixels which contain a number representative of the brightness of the wavelength range of the layer. Values close to zero are darker whereas values closer to 255 (in 8-bit data) are brighter. The set of digital numbers from the same pixel in every layer (band) constitutes the "spectral response"; a representation of the magnitude of reflected radiation across all wavelengths sampled (13). A common graphical representation of the spectral response is to plot the magnitude of the reflectance at each wavelength producing a two-dimensional line graph. Peaks in the graph are "reflective" features whereas depressions are "absorption" features (i.e., low reflectance). As opposed to the interpretation of aerial photographs where the information is solely spatial or contextual, the multiple layers (bands) in a hyperspectral image (e.g., can be over 100 bands) (14,15) contain other information about the surface (e.g., chemical composition) that may be interpreted from the spectral responses. Therefore, not only is the spatial information present in the image, but it is enhanced by the spectral information contained in the multiple bands. Materials both natural (i.e., water, vegetation, soil, rock, etc.) and man-made (i.e., concrete, ceramic, etc.) have different spectral signatures that can be used to identify the type of material or target or even obtain more detailed information about the material, such as its mineral composition, vegetation type and health, paint type, construction material type, etc. (13). This is because the spectral signature is a product of a material or surface's composition, texture, or topography (and/or grain size), and moisture content (16). In most cases, pixels from satellite and airborne imagery represent complex mixtures of the spectral signatures of several targets/surfaces that make up the spatial extent of the pixel unless the area of the pixel is smaller than the unique target/surface of interest. In the former case, there may be pixels that have pure or nearly pure representations of the spectral signatures and can be referred to as "endmembers," signatures from only one target/surface of interest without mixing (15,17).

In this study, we compare the spectral signature of an experimental animal proxy mass grave to that of a false grave over a period of 16 months from *in situ* spectral measurements collected with a field portable spectroradiometer. We also examined an airborne hyperspectral image acquired 1 month following burial to determine whether a grave during and following the decomposition of the bodies reflects electromagnetic radiation differently from the landscape and other disturbances that contextually resemble a grave (e.g., false grave or exposed soil).

Methods

Study Area and Experimental Set-Up

The study area is located in north-western Costa Rica in a tropical moist forest ecosystem at an elevation of 300 m (18). The tropical moist forest ecosystem is characterized by 2000–4000 mm of seasonal precipitation per year, an average temperature greater than 17°C, and a potential evapotranspiration ratio of 0.5–1.0; it comprises 40% of the tropics (19,20). The choice of ecosystem type was important to conduct the experiment in an area with comparable climate to areas with a documented history of disappeared persons and mass graves such as in Guatemala.

Transitions in land management practices over the years by a succession of land owners have resulted in extensive areas of cleared forest to enter into unmanaged regeneration in our study area (18). The experimental mass grave was created in an abandoned pasture that is surrounded by secondary forest to the north and south, old growth forest to the east, and a mosaic of pasture and secondary forest to the west (18). The pasture is covered by inhibitory, aggressive grasses, *Hyparrhenia rufa* (Bergius) and *Paspalum conjugatum* (Nees) (18). Figure 1 illustrates the study site. The soil is described as a medium fertility Inceptisol, type Andic Ustic Humitropet, a common soil type in the tropics (21). These soils have a clayey texture with a low concentration of P and Mg. They have some allophone from the influence of past volcanic ash depositions that rejuvenated the A horizon (i.e., reason for the Andic classification
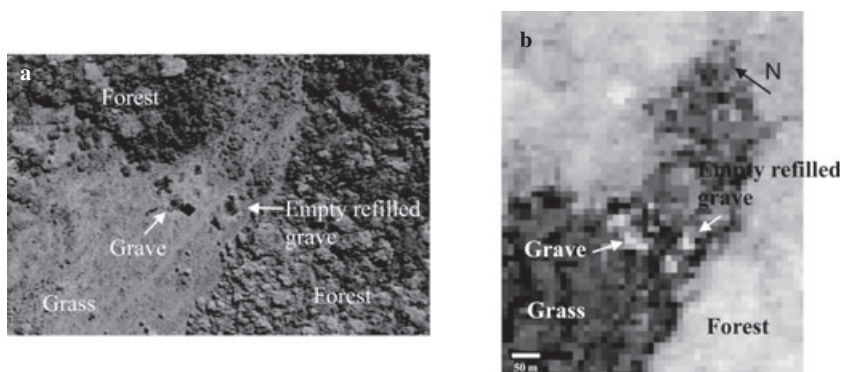

FIG. 1—*(a) High resolution infrared photograph of the experimental site indicating the location of the grave and refilled empty grave. The black square next to the grave is a calibration panel. (b) Airborne hyperspectral image of the experimental site, 4.7 m spatial resolution.*

in the taxonomic name). Taking soil classification into consideration is important because the physical and chemical properties of the soil are a factor in any change in reflectance that may be seen following subsurface cadaveric decomposition.

As described by Kalacska and Bell (22), two $5 \times 5 \times 1.5$ m holes were dug during the last week of February 2005 with a motorized backhoe. The purpose was to create two identical features/graves as this represents the most confounding detection problem. The carcasses of eight free-range antibiotic-free juvenile cattle, total weight *c.* 750–800 lbs (340–363 kg), were purchased from a local slaughterhouse. Organic, free-range livestock was used to avoid a sterilized upper intestinal tract, a chronic outcome of long-term antibiotic use, as this would negate the bacterial overgrowth characteristic of whole body decomposition at the stage of "bloating" and beyond (23,24). The animals were killed on site by blunt force trauma to the head and immediately placed in two rows of four in one of the grave features. Within 2 h the backfill was systematically replaced with the same motorized backhoe and operator interring the carcasses. All other graves were refilled in the same manner. Any remaining soil was leveled within the experimental grave excavation site, and it was not artificially compacted or mounded.

Description of In Situ *Spectral Measurements*

The spectral response of the grave and the false grave was measured with an ASD Fieldspec FR handheld spectrometer (Analytical Spectral Devices, Boulder, CO) within 2 h following burial. This spectrometer measures reflected radiation from 350 to 2500 nm. The purpose of this measurement was to establish a baseline and ensure that any differences seen as the carcasses decompose are not artifacts of differences in the soil that was excavated from and replaced in the grave and the false grave. One month following burial (March 2005), the spectral measurements were repeated (22). Five and 16 months following burial (July 2005, June 2006), the spectral response was measured with an ASD Fieldspec Handheld spectrometer (Analytical Spectral Devices). This spectrometer measures reflected radiation from 325 to 1075 nm. For both the grave and the false grave, all measurements were collected in a grid sampling scheme with 50 spectra collected (i.e., five rows of 10 measurements). The field of view of both instruments was *c.* 4 cm diameter (22) (sampling distance of *c.* 18 cm) and all measurements were collected on clear sunny days. The integration time of both instruments was set using a 99% reflective Spectralon™ industry standard white reference panel (Labsphere, North Sutton, NH). The Spectralon™ panel is a Lambertian surface, therefore its reflectance is diffuse and under the same lighting conditions as the samples, the panel is the brightest surface the instrument sees. A standard "dark current correction" was applied to eliminate instrument noise from spectral measurements (i.e., remove any interference from the instrument itself). White reference measurements, which measure the reflectance of the Spectralon™ panel, were repeated after every 10 sample points from the grave and false grave. These measurements of the Spectralon™ panel are important because reflectance is calculated as the ratio of each measured spectrum of the grave or false grave to the white reference spectrum. Prior to analysis, measurements at wavelengths with high instrument noise from the ASD Handheld spectrometer (below 400 nm and above 900 nm), were removed from all the spectra. The same spectral range is used for the data collected with the ASD Fieldspec FR (i.e., data below 400 nm and above 900 nm were omitted from the analyses). In summary, for each time period (immediately following burial, 1, 5, and 16 months following burial) the data set consists of 50 sampled points that cover the 400–900 nm range. The field of view of the instruments did not overlap between measurements. For the analysis, each measured spectrum is treated as a unique sample point.

Description of Airborne Hyperspectral Image

We also examined airborne hyperspectral imagery collected on March 30, 2005 (1 month following burial) with the HyMap II sensor (Hyvista, North Ryde, NSW, Australia) onboard a WB57 aircraft over a set of three flight lines. The spatial resolution of the imagery is 4.7–5.2 m and contains 125 bands in the 450–2500 nm range (25). A geocorrection was applied to the imagery by Hyvista using their in-house processing software. Hyvista provided the imagery as radiance ($\mu W/cm^2 \ast sr \ast nm$) and as surface reflectance calculated from an atmospheric correction with Hyvista's in-house software. In this study we used the reflectance image because our field measurements are also reflectance measurements and because spectral features are more readily interpretable from reflectance data as opposed to radiance.

In Situ *Spectral Analysis*

A fourth order polynomial Savitsky–Golay smoothing filter (26) with a window size of 41 was applied to the *in situ* spectra from all four time periods. With spectral bands spanning the 400–900 nm range, the *in situ* data have 500 dimensions (i.e., each wavelength from 400 to 900 represents one dimension). While hyperspectral data contain substantial information in the narrow contiguous bands, the data have different geometric and statistical properties in comparison to conventional two- or three-dimensional data (27). As the number of dimensions increases, the amount of data necessary to properly estimate multivariate class densities also increases; in our analysis we have two "*classes*" of interest, the grave and the false grave. Reducing the dimensions of the data from 500 to an "*optimal number of dimension (bands)*" is important because it removes any redundant bands, makes the analysis more manageable logistically and reduces the data to only the bands that contain the most important information for separating the spectra of the grave from the false grave (27). A technique called "forward feature selection" (28,29) was thus applied to reduce the dimensionality of the *in situ* data. In this technique initially all 500 bands are examined to locate the best one for separating the classes based on the nearest neighbor (NN) criterion. The process is iterative as bands are added in the order they maximize the criterion function (J). If the set of currently selected bands is represented by X_{di}, the criterion function $J_j = J (X_{di} + \xi_j)$ is evaluated and bands are added to the optimal set (ξ_j) in the order they most improve the value of J_j (30). We examined the top 10, 20, and 30 bands. The theoretical maximum number of bands that can be used in the classification approach that was employed after the best bands were chosen can be calculated from $F = (n - g)/3$ where F is the maximum number of bands, n is the number of spectra available, and g is the number of groups or classes (31). The end result of the forward feature selection is a new dataset with a reduced number of dimensions (i.e., 10–30 bands instead of the original 500) that are the most effective at discriminating between the grave and the refilled disturbance (false grave). At this point in the analysis, there is neither the measure of how well the reflectance of the grave and the false grave can be classified, nor an indication of which classifier is best. The next step in the analysis was to train specific classifiers to separate the reflectance of the grave and false grave. Each classifier uses a different learning

methodology and constructs different decision boundaries. This provides a measure of how well they classify (separate) the reflectance spectra of the two classes.

A set of standard nonparametric classifiers were examined to differentiate the reduced spectra obtained from the forward feature selection (29). The classifiers we examined were a binary decision tree (*treec*), a feed forward neural network using the Levenberg–Marquardt optimization with two to five layers (*lmnc 2–5*)(32) and the k-NN classifier which predicts the class membership of a data point based on the class of its "k" nearest neighbours in feature space (29). For this analysis we examined the two and three NNs (*knnc 2–3*). The data were divided equally into training and validation datasets with labels were being supplied to indicate class membership. The training dataset was used to train the classifiers and provide an error estimate while the validation dataset provided an indication of how well each classifier discriminated between the two classes. The optimal number of bands (10, 20, or 30) to use with each classifier was determined by examining the training and validation errors for each of the 10, 20, and 30 band sets. The point at which the two error estimates were at a minimum was the optimal number of bands for each classifier (33). Finally, to facilitate the interpretation of the classification results, the relative separability at each wavelength was mapped with the Bhattacharyya test statistic which identifies the areas with the minimum attainable classification error (34,35). All analyses were conducted with Matlab v.7 release 14 (The MathWorks, Natick, MA) and PRTools 2004 (Delft Pattern Recognition Group, Delft, The Netherlands) (29).

Airborne Image Analysis

The flight lines from the HyMap II sensor were subset to a 2 km^2 area surrounding the experimental site. A minimum noise fraction (MNF) transform (36–38) was applied to the imagery to reduce the number of bands (i.e., dimensions) from the original 125 bands to 20 uncorrelated bands. This implementation of the MNF algorithm after Green et al. (37), consists of two principal component transformations. The first one estimates the amount of noise in the data and subsequently decorrelates (i.e., results in a transformed data set where there are no band to band correlations) and rescales the noise while the second is a standard principal component transform. The resultant bands which contained coherent data were examined in multidimensional space to assess the separability of the grave versus other targets in the imagery, namely, the false grave, exposed soil, pasture grass, and forest. All image analyses were conducted in ENVI v4.1 (ITT Visual Information Solutions, Boulder, CO).

Results

In Situ *Spectra*

The spectral signatures of the experimental grave and control were not reliably separable with the range of classifiers with any number of features immediately following burial (i.e., within 2 h after burial); the overall error rate ranged between 15% and 35%. This indicates that the grave and the false grave have a similar baseline spectral response (determined by the chemical composition, organic material content, texture, water content, and grain size).

1-Month Interval

One month following burial (March), the spectra of the grave and false grave resembled each other visually with small deviations in amplitude and shape; the amplitude of the false grave spectra had a higher reflectance in the red and near infrared regions (Fig. 2). Neither the grave nor the false grave had any regenerating vegetation. Because both the creation of the grave in February and this measurement in March took place in the dry season, there had been no precipitation at the site. Results from the pattern classifiers indicate that even with the apparent visual similarity of the spectra, near perfect separability (0% training error; 1.9% testing error; 0.95% overall error) was achieved with the *lmnc4* and *lmnc5* classifiers (see Methods section for classifier descriptions) using the 10 optimal bands. The *lmnc3* classifier had the third lowest error with overall error of 1.95% (0% training error; 3.9% testing error). The Bhattacharyya test statistic (Fig. 3) illustrates the regions with the greatest separability as the visible region from 400 to 550 nm and in the near infrared above 850 nm. This is consistent with the ranges from which the top 10 bands used in the classification were chosen through the forward feature selection.

5-Month Interval

Five months following burial (July), the study area experienced two and a half months of intermittent precipitation. Vegetation growth and regeneration in this ecosystem is vigorous in the rainy season, and therefore, it was expected that both the false grave and the grave would have undergone natural vegetation regeneration processes (21,39). However, as can be seen from the photographs in Fig. 2, the false grave is *c.* 60% vegetated with grasses while the grave remains vegetation free. Analysis of the spectra for this time period is included for completeness. The spectra of the false grave, although highly variable, began to resemble the spectral response characteristic of vegetation (40), while the spectra of the grave continue to be representative of soil (16,41) (Fig. 2). As expected, perfect separability is achieved with the *lmnc3* and *knnc2* classifiers while *lmnc2*, *lmnc5*, and *knnc2* achieved 1% overall error (0% training error; 2% testing error). The Bhattacharyya test statistic highlights a narrow peak around 450 nm and a broad peak around 550 nm as the areas with the greatest separability between the grave and false grave (Fig. 3), again consistent with the ranges from the feature selection. The region centered on 550 nm, the *green peak* in vegetation spectra is representative of photosynthethic pigments, such as chlorophylls *a* and *b* and photoprotection pigments such as those associated with the xanthophyll cycle (42–45). Soil spectra do not exhibit this characteristic feature (16) as can be seen in Fig. 2 when comparing the mean spectral signatures of the grave and the false grave for the 5-month time period. The plateau in the near infrared region, apparent in the spectral signature of the false grave (Fig. 2), is also a characteristic of vegetation spectra (40). Healthy green vegetation tends to have strong absorption in the red wavelengths and high reflectance in the near infrared. The inflection point between the two is referred to as the *red-edge* and can be related to foliar nitrogen and chlorophyll content (46). The near infrared plateau of vegetation reflectance is predominantly controlled by internal structure at the leaf level (40,47) and is also influenced by leaf area index, water content, plant physiology, and stress at the canopy level (47).

16-Month Interval

Sixteen months following burial (June), the study site has experienced an entire rainy season (May 2005 to January 2006), a second dry season (February to April 2006), and one month and a half of a second rainy season (May to June 2006). Regeneration of the
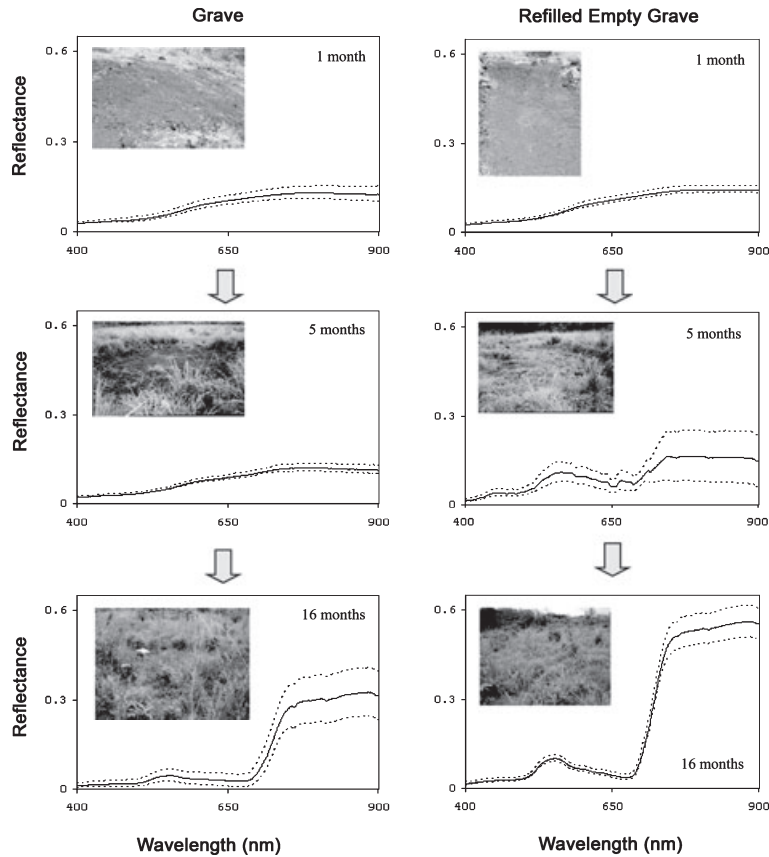
FIG. 2—*Progression of the spectral signatures of the experimental animal mass grave and the false grave over 16 months from the* in situ *hand-held measurements. Mean is indicated by a solid line, standard deviation by dotted lines.*
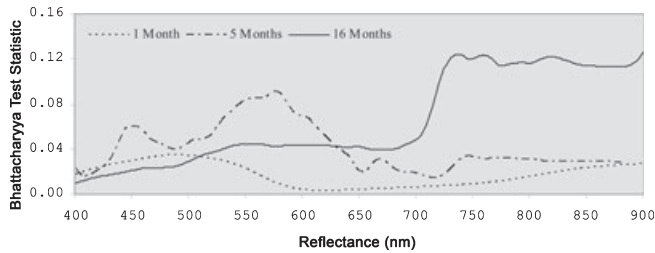

FIG. 3—*Bhattacharrya's test statistic indicating the areas of the spectrum with the greatest separability between the reflectance of the experimental animal mass grave and the false grave, 1, 5, and 16 months following burial from the* in situ *hand-held measurements.*

pasture grasses is expected to be complete on both the grave and the false grave. Regeneration can be seen on the grave, although *c.* 30% remains vegetation-free around the edges (Fig. 2). Conversely, the false grave can no longer be distinguished from the undisturbed pasture (Fig. 2). The mean spectral response of both the grave and false grave is that of vegetation (Fig. 2) that provides a valid spectral comparison. The false grave clearly has a higher reflectance in the green peak and the near infrared plateau as well as stronger absorption in the red wavelengths (Fig. 2). The Bhattacharyya test statistic indicates that optimal regions for differentiating the spectra are the near infrared plateau above 700 nm with fairly reasonable separability in the 550–700 nm region as well, corresponding with the forward feature selection results. Perfect separability was achieved with the *lmnc2*, *lmnc3*, *lmnc4*, and *knnc2* with 1.19%

overall error for *lmnc5* and *treec* (0% training error; 2.38% testing error).

Hyperspectral Airborne Imagery

Representative spectra of the grave, false grave, pasture grass, and forest from the HyMap II imagery are shown in Figs. 4*a* and 4*b*, while the experimental site is illustrated in Fig. 1. The best separation in *n*-dimensional space between the grave and all other targets in the imagery is with the top nine eigenimages from the forward MNF transform with the exception of eigenimage 7 which did not contribute to the separability (Fig. 5). The forest class is the most dissimilar, while the two classes closest in *n*-dimensional space to the grave are the false grave and dry grass, as expected.

Discussion

Our results demonstrate that the reflectance spectra of the grave are readily distinguishable from soil disturbance (i.e., false grave) throughout the entire 16 months after burial using *in situ* hyperspectral data. This time period (16 months) is representative of instances where both the grave and false grave are in a purely "exposed soil" state (1 month following burial), a "transitional mixture" of vegetation and exposed soil (5 months following burial), and "vegetated" (16 months following burial). From airborne imagery collected 1 month following burial, the spectra of the grave also showed a clear separation from the other classes in the imagery in *n*-dimensional space.
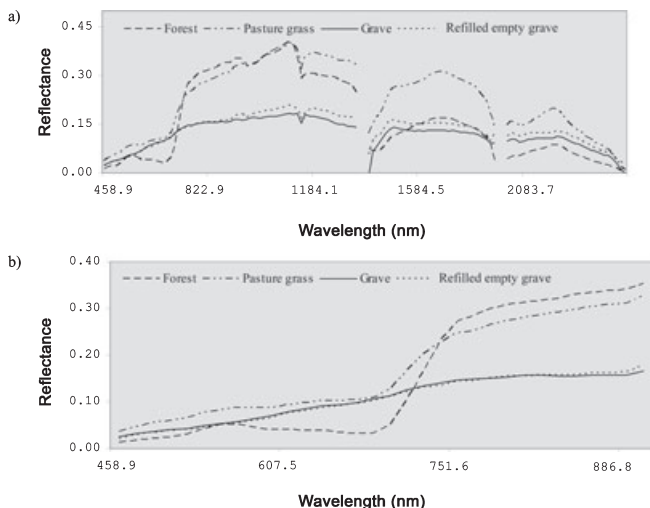
FIG. 4—(a) Mean spectra of the grave, false grave, pasture grass, and forest from the hyperspectral airborne image (4.7 m spatial resolution) over the entire 125 bands and (b) same spectra as in (a) truncated to the 458.9–901.8 nm range.
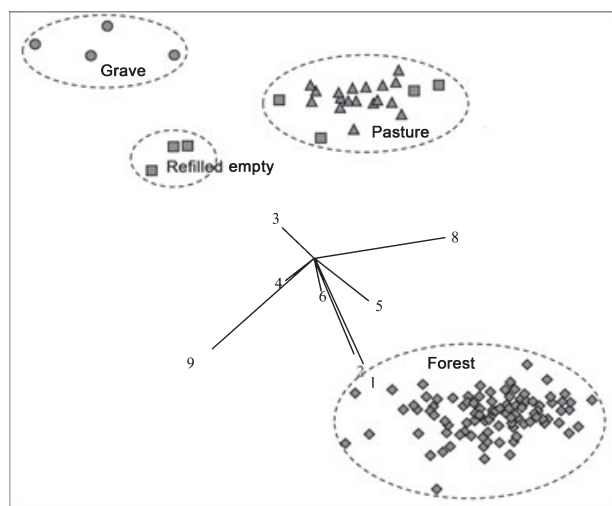

FIG. 5—Eight dimensional scatter plot of the spectral signatures of pixels representing the grave versus the false grave, grass, and forest following the forward minimum noise fraction (MNF) transform. Notice that the mass grave containing bodies is clearly separable from other classes. The spectra are from the airborne hyperspectral image. Each point represents one pixel.

As a form of machine learning, the pattern classifiers adapted to new data to detect and extrapolate patterns (48). This ability and the feature selection were the key for identifying the most distinct spectral regions and discriminating the spectra of the grave during the sampling intervals when the spectra of the grave and false grave were very similar, namely, 1 and 16 months following burial (Fig. 2). Focusing on a few specific narrow bands facilitated the separation for all time periods, especially when shape and amplitude were similar.

During vegetation regeneration, the spectral properties of the vegetation provide additional insight into the detection of clandestine graves. Because vegetation will ultimately obscure grave sites fairly quickly in most environments, investigating the underlying basis for the spectral differences is an important question. It is shown by Calvo-Alvarado et al. (49) that the reflectance spectra of blades of the *P. conjugatum* growing on the grave and in the pasture measured

at the 16-month interval differ and can be separated with the pattern classifiers perfectly. The time frame for which this difference in the vegetation spectra lasts, is yet to be determined. In an analysis of the soil chemistry, Calvo-Alvarado et al. (49) showed significant differences in multiple elemental concentrations (e.g., N, S, C, Mn among others) between samples from the grave and the false grave, collected 16 months after burial, which will influence the reflectance of the regenerating vegetation (50). Over 80 volatile organic compounds resulting from the decomposition of the human body have been identified (51), a number of which have also been shown to be detectable at the surface of experimental graves over a period extending from burial to 4 years (52). Among the most prominent are dimethyl disulfide ($C_2H_6S_2$), toluene (C_7H_8), hexane (C_6H_{14}), benzene 1,2,4-trimethyl (C_9H_{12}), cadaverine ($C_5H_{14}N_2$), and putrescine ($C_4H_{12}N_2$) (51,53). These and other decomposition compounds in the soil may have inhibited vegetation regrowth by creating an initially toxic environment for vegetation, soil microbes, and micorrhizae, explaining the lack of vegetation 5 months following burial and the incomplete vegetation cover 16 months postburial on the grave. These differences in soil chemistry must also influence the overall difference in the spectral response of the grass as shown by Calvo-Alvarado et al. (49). Similar differences in vegetation regrowth and soil elemental concentrations have been shown elsewhere, during surface cadaveric decomposition (50). The heat and water vapor produced during decomposition condenses when reaching the surface, thus precipitating the soluble cations, salts, and other toxic compounds. This movement of the vapor is facilitated by the excavation itself, and subsequent refilling which decreases the compaction and increases soil porosity. Following dissipation of the toxicity, it may be speculated that the soil becomes enriched either through the translocation of nutrients or via the liberation of nutrients present in the soil colloids at the interlayers (2:1 clays and allophane in this case) because of the increased temperature and gas/water vapor emission. For example, Calvo-Alvarado et al. (49) showed that sulfur concentration is nearly double from the grave as from the false grave.

Organic compounds have a high rate of adsorption in clay-based soils (such as the Inceptisol from the study area) thus adhering to the soil particles, resisting leaching (54). Some of the compounds produced during decomposition such as benzene and toluene (hydrocarbons) are common soil contaminants from, say, underground fuel tank ruptures. Even at low concentrations, hydrocarbon contamination has been shown to have adverse effects on the metabolism of soil microbes and plants (55). Carter et al. (50) indicate that surface cadaveric decomposition can alter the soil chemistry and vegetation for up to 10 years, therefore, it is plausible that the differences seen 1 month following burial in the soil spectra and in the vegetation spectra 16 months following burial are a result of the subsurface cadaveric decomposition, mainly from the soft tissues. However, the changes in the chemistry of subsurface mass graves through time remain largely unstudied with only anecdotal observations of spatial variability of body preservation (56–60).

An important consideration for future studies is to examine the effect of spatial resolution, especially in the choice of imagery. In this study, the spatial resolution achievable by airborne hyperspectral sensors (5 m) was found to be sufficient for the detection of a mass grave that covers an area of 25 m^2. This same data would also be applicable to larger sites where several pixels would represent the grave. For buried landmine detection, a problem analogous to the detection of graves, it was found that a resolution finer than half of the burial scar did not improve discrimination accuracy using hyperspectral data (61,62). Additional studies are necessary to examine data with a coarser spatial resolution such as imagery from civilian hyperspectral satellite sensors (e.g., 17 m for the

PROBA-CHRIS sensor). At that scale, each pixel is a nonlinear mixture of multiple elements, posing a subpixel problem which, though not impossible, results in a more complicated analysis. The detectability of graves approximately the same size as examined here (i.e., 5×5 m) would be dependent upon the surrounding environment and the amount of mixing within the pixels. As a general guideline, minimal mixing between the grave and the spectral response of other elements within the pixels, and maximal dissimilarity between the spectral response of the grave and the other elements within each pixel enhances the potential for detection.

In addition, based on our results, hyperspectral data is crucial for highest accuracy in detecting the graves. It is unlikely that data from high spatial resolution (e.g., 2 or 4 m) multispectral sensors with four broad spectral bands would result in the same accuracy (i.e., low error) for detecting the graves. Such sensors are sufficient for separating exposed soil from other cover types such as vegetation or urban features, but the spectral resolution of the broad bands does not have the detail needed to discriminate between a grave containing cadavers and other types of soil disturbance. As shown here, very specific narrow bands are needed to discriminate between the spectral response of the grave and disturbed soil with the lowest error.

Additional considerations include the effect of time and environment. Our results show successful discrimination over a 16-month period from a tropical moist forest environment that experiences seasonal precipitation. Because vegetation is highly responsive to its environment, these influences are relayed through its spectral properties. As the soil effects dissipate over time, differences in the spectral response of vegetation may also dissipate. However, because the chemical changes within a mass grave through time have not been studied, it is unknown whether changes in the soil environment may linger for several years or decades as shown by Carter et al. (50) for surface decomposition. By applying the methodology presented in this study to several actual mass graves of varying ages and in varying environments, the questions regarding the effects of time may begin to be resolved. Investigating the transferability of our results to other ecosystems is necessary to address both a wider applicability of these methods within and outside the tropics and also to identify the commonalities and differences in the results found in other ecosystems. For example, in dry ecosystems with little to no vegetation, the focus of the analysis must be on the differences in the reflective and absorptive properties of the substrate (i.e., soil, sand, etc.) as in the results 1 month following burial in this study. Differences in the spectral properties of the substrate may then be traced back to changes in the chemical composition, mineral structure, grain size, water content, surface texture, etc. of the substrate to better understand the differences in reflectance. While in a temperate environment, for example, the effect of the freeze-thaw cycles on decomposition must also be taken into consideration.

We demonstrate that the spectral information inherent in a hyperspectral image provides the fundamental objective information that can assist the detection of mass graves. By relying solely on the spatial context and shapes of objects as one would with an aerial photograph or panchromatic image, the shapes and context of objects may be attributed to alternatives for soil disturbance. With such data, graves cannot be objectively distinguished from other alternatives as seen in the high resolution aerial photograph in Fig. 1. Without consideration of the spectral domain, the objective view provided by imagery (airborne or satellite) therefore becomes subjective and dependent upon the experience and personal biases of the interpreter. By taking into account the spectral information, however, the analysis becomes an objective assessment of the data,

and as we have shown, a successful tool for locating possible mass burials. The final proofing that the mammal decomposition signal is human requires that the feature is excavated in the normal way, as no unique chemical human identifier is currently known (52).

Conclusions

The results from this study represent a real breakthrough in the remote detection of clandestine mass graves. We found distinct differences in the spectral signature of a simulated grave that contained mammalian carcasses to that of a false grave from *in situ* spectrometry over a 16-month period following burial. We also identified distinct spectral differences from airborne hyperspectral imagery 1 month following burial. With further development, airborne hyperspectral imagery could be used as a rapid first-look to detect and confirm the existence of suspicious decomposition signatures, i.e., mass graves. This study has demonstrated that fly-over and potentially satellite hyperspectral imagery provides a new detection tool for the international community. Furthermore, the location of graves is one of the first steps in organizing a recovery team to exhume and identify the remains for the purpose of evidence collection for prosecution and for the return of individuals to families. Remotely sensed data comprises evidence in its own right which is scientifically defensible and therefore, an instrument for domestic or international legal process and justice.

References

1. FAFG. Fundacion de Antropología Forense de Guatemala. Guatemala, 2006. Available from http://www.fafg.org. Accessed November 12, 2008.
2. Melvern L. Conspiracy to murder. New York: Verso, 2004.
3. Kumar R. Divide and fall? Bosnia in the annals of partition. New York: Verso, 1997.
4. Khan SM. The shallow graves of Rwanda. New York: I.B. Tawns & Co., 2001.
5. Totten S, Parsons WS, Charny IW. Century of genocide. New York: Routledge, 2004.
6. Jessee E, Skinner M. A typology of mass grave-related sites. Forensic Sci Int 2005;152:55–9.
7. Skinner M, Sterenberg J. Turf wars: authority and responsibility for the investigation of mass graves. Forensic Sci Int 2005;151:221–32.
8. Skinner M, Alempijevic D, Djuric-Srejic M. Guidelines for international forensic bio-archaeology monitors of mass grave exhumation. Forensic Sci Int 2003;134:81–92.
9. Cordner S, Coupland R. Missing people and mass graves in Iraq. Lancet 2003;362:1325–6.
10. Dallaire R, Power S. Shake hands with the devil: the failure of humanity in Rwanda. New York: Carroll & Graf, 2004.

11. McGray D. Unearthing grave offenses. Foreign Policy 2001;126:86–7.
12. Juhl K, Olsen OE. Societal safety, archeology and the investigation of contemporary mass graves. J Genocide Res 2006;8(4):411–35.
13. Showengerdt RA. Remote sensing: models and methods for image processing. 3rd ed. New York: Academic Press, 2007.
14. Landgrebe DA. Signal theory methods in multispectral remote sensing. New York: Wiley-Interscience, 2003.
15. Chang C-I. Hyperspectral imaging techniques for spectral detection and classification. New York: Kluwer Academic Publishers, 2003.
16. van der Meer F. Physical principles of optical remote sensing. In: Stein A, van der Meer F, Gorte B, editors. Spatial statistics for remote sensing. Boston: Kluwer Academic Press, 1999;27–40.
17. Wang J, Chang CI. Applications of independent component analysis in endmember extraction and abundance quantification for hyperspectral imagery. IEEE Trans Geosci Remote Sens 2006;44(9):2601–16.
18. Kalácska M, Sánchez-Azofeifa GA, Rivard B, Calvo-Alvarado JC, Journet ARP, Arroyo-Mora JP, et al. Leaf area index measurements in a tropical moist forest: a case study from Costa Rica. Remote Sens Environ 2004;91:134–52.
19. Holdridge LR. Life zone ecology. San José, Costa Rica: Tropical Science Center, 1967.
20. UNEP-Caribbean Environmental Programme. Status of protected area systems in the wider Caribbean region, Guatemala: UNEP, 1996, Technical Report No. 36.
21. Holdridge L, Grenke WC, Hatheway WH, Liang T, Tosi J Jr. Forest environments in tropical life zones: a pilot study. New York, NY: Pergamon, 1971.
22. Kalácska M, Bell LS. Remote sensing as a tool for the detection of clandestine mass graves. Can Soc Forensic Sci J 2006;39(1):1–13.
23. Gilbert P, McBain AJ. Potential impact of increased biocides in consumer products on prevalence of antibiotic resistance. Clin Microbiol Rev 2003;16(2):189–208.
24. Simpson CK, Knight B. Forensic medicine. 9th ed. London, UK: Edward Arnold, 1985;6–18.
25. Cocks T, Jenssen R, Stewart A, Wilson I, Shields T, editors. The Hymap airborne hyperspectral sensor: the system, calibration and performance. 1st EARSEL Workshop on Imaging Spectroscopy; Zurich, Switzerland, Oct 6–8, 1998. Strasbourg, France: European Association of Remote Sensing Laboratories, 1998;37–42.
26. Orfanidis SJ. Introduction to signal processing. Englewood Cliffs, NJ: Prentice-Hall, 1996.
27. Jimenez LO, Landgrebe D. Supervised classification in high-dimensional space: geometrical, statistical, and asymptotic properties of multivariate data. IEEE Trans Syst Man Cybern C Appl Rev 1998;28(1):39–54.
28. Duin RPW. PRTools v.3.0—a matlab toolbox for pattern recognition. 3.0 ed. Delft, The Netherlands: Delft Institute of Technology, 2000.
29. van der Heijden F, Duin RPW, de Ridder D, Tax DMJ. Classification, parameter estimation and state estimation: an engineering approach using MATLAB. West Sussex, UK: John Wiley & Sons Ltd., 2004.
30. Webb A. Statistical pattern recognition. 2nd ed. West Sussex, England: Wiley, 2002.
31. Defernez M, Kemsley EK. The use and misuse of chemometrics for treating classification problems. TrAc Trends Analyt Chem 1997; 16(4):216–21.
32. Hagan MT, Menhaj M. Training feed-forward networks with the Marquardt algorithm. IEEE Trans Neural Networks 1994;5:989–93.
33. Fielding AH, editor. Machine learning methods for ecological applications. Berlin/Heidelberg, Germany: Springer, 1999.
34. Chernoff H. A measure of asymptotic efficiency for tests of a hypothesis based on the sum of observations. Ann Math Stat 1952;23:493–507.
35. The MathWorks. Bioinformatics toolbox reference for use with MATLAB. 2nd ed. The MathWorks (updated 2006; cited). Available from: http://www.mathworks.com/access/helpdesk/help/toolbox/bioinfo. Accessed November 12, 2008.
36. Boardman JW, Kruse FA, editors, Automated spectral analysis: a geological example using AVIRIS data, North Grapevine Mountains, Nevada. ERIM Tenth Thematic Conference on Geologic Remote Sensing, San Antonio, TX, May 9–12, 1994. Ann Arbor, MI: Environmental Research Institute of Michigan, 1994; 23–6.
37. Green AA, Berman M, Switzer P, Craig MD. A transformation for ordering multispectral data in terms of image quality with implications for noise removal. IEEE Trans Geosci Remote Sens 1988;26(1):65–74.
38. Underwood EC, Ustin SL. A comparison of spatial and spectral image resolution for mapping invasive plants in coastal California. Environ Manage 2007;39:63–83.
39. Webb LJ, Tracey JG, Williams WT. Regeneration and pattern in the subtropical rain forest. J Ecol 1972;60:675–95.
40. Gates DM, Keegan JC, Schleter VR, Weidner VR. Spectral properties of plants. Appl Optics 1965;4:11–20.
41. Dematte JAM, Campos R, Alves M, Fiorio PR, Nanni M. Visible-NIR reflectance: a new approach on soil evaluation. Geoderma 2004;121 (1-2):95–112.
42. Guo J, Trotter CM. Estimating photosynthetic light-use efficiency using the photochemical reflectance index: variations among species. Funct Plant Biol 2004;31:255–65.
43. Stylinski CD, Gamon JA, Oechel WC. Seasonal patterns of reflectance indices, carotenoid pigments and photosynthesis of evergreen chaparral species. Oecologia 2002;131(3):366–74.
44. Sims DA, Gamon JA. Relationships between leaf pigment content and spectral reflectance across a wide range of species, leaf structures and developmental stages. Remote Sens Environ 2002;81(2-3):337–54.
45. Gamon JA, Penuelas J, Field CB. A narrow-waveband spectral index that tracks diurnal changes in photosynthetic efficiency. Remote Sens Environ 1992;41:35–44.
46. Cho MA, Skidmore AK. A new technique for extracting the red edge position from hyperspectral data: the linear extrapolation method. Remote Sens Environ 2006;101:181–93.
47. Asner GP. Biophysical and biochemical sources of variability in canopy reflectance. Remote Sens Environ 1998;64:234–53.
48. Russell S, Norvig P. Artificial intelligence: a modern approach. 2nd ed. Upper Saddle River, NJ: Prentice Hall, 2003.
49. Calvo-Alvarado JC, Kalacska M, Sanchez-Azofeifa GA, Bell LS. Effect of soil type on the reflectance of tropical tree and grass species. In: Kalacska M, Sanchez-Azofeifa GA, editors. Hyperspectral remote sensing of tropical and subtropical forests. New York: Taylor and Francis Group, CRC Press, 2008; 87–123.
50. Carter DO, Yellowlees D, Tibbett M. Cadaver decomposition in terrestrial ecosystems. Naturwissenschaften 2007;94(1):12–24.
51. Statheropoulos M, Spiliopoulou A, Agapiou A. A study of volatile organic compounds evolved from the decaying human body. Forensic Sci Int 2005;153:147–55.
52. Vass AA, Smith RR, Thompson CV, Burnett MN, Dulgerian N, Eckenrode BA. Odor analysis of decomposing buried human remains. J Forensic Sci 2008;53(2):384–91.
53. Vass AA, Barshick SA, Sega G, Caton J, Skeen JT, Love JC, et al. Decomposition chemistry of human remains: a new methodology for determining the postmortem interval. J Forensic Sci 2002;47:542–53.
54. Khan Z, Anjaneyulu Y. Selection of hazardous waste dumpsites based on parameters effecting soil adsorption capacity—a case study. Environ Geol 2003;43(8):986–90.
55. Hogan M, Patmore L, Latshaw G, Seidman H. Computer modeling of pesticide transport in soil for five instrumented watersheds. Athens, GA: U.S. Environmental Protection Agency Southeast Water Laboratory, 1973.
56. Dent BB, Forbes SL, Stuart BH. Review of human decomposition processes in soil. Environ Geol 2004;45:576–85.
57. Mant AK. A study of exhumation data. London, UK: University of London, 1950.
58. Haglund WD, Connor MA, Scott DD. The archeology of contemporary mass graves. Hist Archaeol 2001;35(1):57–69.
59. Bell LS, Skinner M, Jones SJ. The speed of postmortem change to the human skeleton and its taphonomic significance. Forensic Sci Int 1996;82:129–40.
60. Haglund WD. Recent mass graves, an introduction. In: Haglund WD, Sorg MH, editors. Advances in forensic taphonomy, method, theory and archeological perspectives. New York, NY: CRC Press, 2002; 243–61.
61. Smith AM, Kenton AC, Horvath R, Nooden LS, Michael J, Wright JA, et al. Hyperspectral mine detection phenomenology program. Proc SPIE Int Soc Opt Eng 1999;3710(2):819–29.
62. Kenton AC, Schwartz CR, Horvath R, Cederquist JN, Nooden LS, Twede DR, et al. Detection of land mines with hyperspectral data. Proc SPIE Int Soc Opt Eng 1999;3710(2):917–28.

Additional information and reprint requests:
Margaret Kalacska, Ph.D.
Department of Geography
McGill University
805 Sherbrooke West
Montreal, QC H3A 1K6
Canada
E-mail: margaret.kalacska@mcgill.ca